ADVANCED THEORY AND SIMULATIONS
www.advtheorysimul.com

Formation of Linear Oligomers in Solid Electrolyte Interphase via Two-Electron Reduction of Ethylene Carbonate

*Yue Liu, Yu Wu, Qintao Sun, Bingyun Ma, Peiping Yu, Liang Xu, Miao Xie, Hao Yang, and Tao Cheng**

Solid electrolyte interphase (SEI) plays a significant role in enhancing the stability and durability of lithium metal batteries (LMBs) by separating highly reactive lithium metal anode (LMA) from the electrolyte to avoid continuous degradation. However, the underlying reaction mechanism is still far from clear. Herein, a hybrid ab initio and reactive force field (HAIR) method is employed to extend the ab initio molecular dynamics (AIMD) to 1 ns, which provides crystal information about the reaction mechanism of elementary reactions that can explain the components and morphology evolution of SEI formation. Specifically, HAIR simulation confirms the two-electron ($2e^-$) reduction of ethylene carbonate (EC) by releasing CO and CO_2, agreeing with phenomenal experiment observation. As the unsaturated intermediates accumulate, polymerization reactions occur, producing linear polyethylene oxide (PEO), $Li_2OCO_2CH_2CH_2$, $Li_2OCO_2(CH_2)_4$, etc., which regulate the formation of outer organic layer (OOL) that consists of linear polyethylene oxide (PEO), $Li_2OCO_2CH_2CH_2$, $Li_2OCO_2(CH_2)_4$, etc., and the inner inorganic layer (IIL) mainly consists of LiF and Li_2O. Simulations at low concentration (LC, 1M) and high concentration (HC, 5M) reveal significantly different reaction pathways when HC electrolyte can significantly promote the formation of homogenous LiF that has been regarded as an important component to facilitate robust SEI.

1. Introduction

Lithium metal batteries (LMBs) have been widely recognized as the most attractive battery architecture for next-generation energy storage, especially for such applications demanding high energy density as electric vehicles (EV), because Li metal owns high voltage (>4.0 V), the excellent theoretical specific energy density of 3860 mAh g^{-1} and volumetric capacity of 2045 mAh cm^{-3}.[1–5] However, commercial uses of LMB on a large scale are still a long way off. Significant challenges that almost killed the interest of Li metal anode in the last 20 years still exist. The high reactivity of lithium metal electrodes, for example, causes constant reduction between electrode and electrolyte, resulting in dendritic development and the formation of heterogeneous solid-electrolyte interphase (SEI) layer.[6,7] Such safety concern induced by dendrite growth has been known as one of the major problems. Another serious obstacle is the insufficient Coulombic efficiency (CE).[8,9] The best-reported system cannot reach the 99.9% CE for a single cycle yet.

Since the relevance between the stability of Li metal electrode and structural or components of SEI layer were clarified,[10,11] extensive works have focused on facilitating optimization of SEI formation process by manipulating the nature of electrolyte.[12–17] The SEI film, derived from the degradation reduction of electrolyte at Li metal anode surfaces, remains unclear because of the complex and heterogeneous sub-structure.[18,19] In recent years, ethylene carbonate (EC), serving as the major component of most electrolytes, has been typically comprised of linear carbonates and lithium bis(trifluoromethanesulfonyl)imide (LiTFSI) salt.[20,21] Thus, the degradation reduction process of EC and LiTFSI is crucial to be elucidated for a comprehensive understanding of the structural and components of multi-layered SEI film.

The complex nature of SEI requires multiscale simulation[22] that is based on accurate DFT calculations.[23] Theoretically, the initial reduction reaction mechanisms of EC have been proposed using density functional theory (DFT) calculations and ab initio molecular dynamics (AIMD) simulations, which play an important role in SEI composition.[22–29] Moreover, a significant amount of CO and C_2H_4 were also detected with a gas chromatography analysis and thermal conductivity detector (GC-TCD), in good agreement with the theoretical results.[30] However, The time scales of AIMD simulations are restricted to hundreds of picoseconds because of the high computing expense. The initial reduction process between Li metal anode and electrolyte EC is

Y. Liu, Y. Wu, Q. Sun, B. Ma, P. Yu, L. Xu, M. Xie, H. Yang, T. Cheng
Institute of Functional Nano and Soft Materials (FUNSOM)
Soochow University
Suzhou 215123, China
E-mail: tcheng@suda.edu.cn

The ORCID identification number(s) for the author(s) of this article can be found under https://doi.org/10.1002/adts.202100612

DOI: 10.1002/adts.202100612

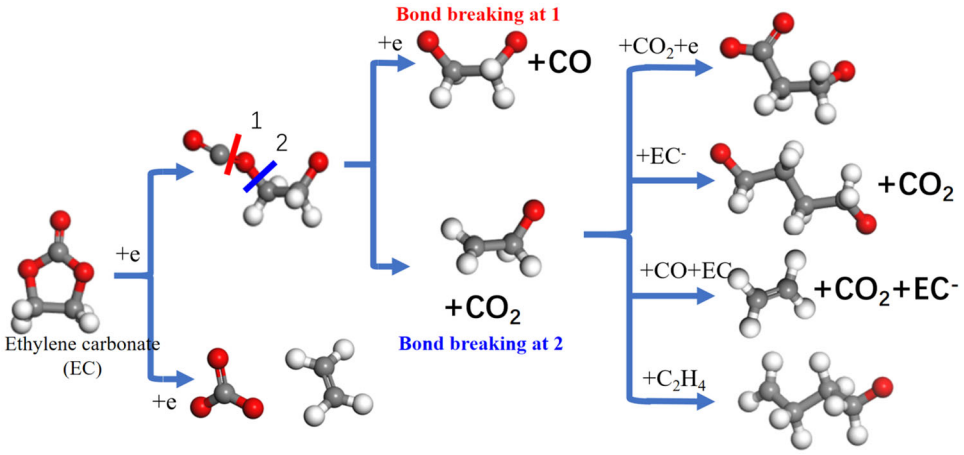

Figure 1. Initial reductive reaction pathways of EC obtained from HAIR simulations.

only sufficient, while SEI formation requires further long-time molecular dynamics (MD) simulations.

Additionally, reactive force field (ReaxFF), a bond-order-depended method, is developed based on quantum mechanics (QM) results, extending the simulation time scale in SEI formation up to millions of atoms for a nanosecond and beyond.[31,32] Bedrov[33] conducted EC neutral molecule and anion reduction process using ReaxFF and QM calculations, $(CH_2CH_2OCO_2Li)_2$ and $(CH_2OCO_2Li)_2$ with the elimination of C_2H_4 are identified as the organic layer. Yun[34] investigated SEI components with the different solvent mixtures, such as EC with dimethyl carbonate (DMC) or ethyl methyl carbonate (EMC). (C_2H_4, CO, CO_2, CH_4, and C_2H_6), and inorganic (Li_2CO_3, Li_2O, and LiF) and organic (ROLi and $ROCO_2Li$: R = $-CH_3$ or $-C_2H_5$) products are observed during ReaxFF MD simulations some of them are detected experimentally.[35]

Unfortunately, the current functional forms of ReaxFF do not include a proper description for explicit electron, which has trouble exploring electron (e^-) transfer reaction during electrochemical processes.[36] Islam and van Duin[37] extend the eReaxFF method to treat electrons explicitly in a pseudo-classical manner, and the major reduction reaction pathways were observed, including electron transfer. These theoretical results suggest the initial reduction process of EC, while long-time simulations for SEI formation are still worthy of being clarified. In addition, due to the lack of LiTFSI ReaxFF parameters, battery-related systems, including LiTFSI, may not be available, implying few related works using ReaxFF are reported, despite their importance.

This work explored the reduction reaction mechanism and SEI formation process via an alternative hybrid scheme, namely, Hybrid ab initio and reactive force field reactive dynamics (HAIR). The hybrid scheme employed the AIMD method to describe accurate localized electrochemical reactions. The longer-range or longer-time chemical reactions with a mass transfer are conducted with ReaxFF in the meantime. The successful hybrid method has been verified, and the LiTFSI-related ReaxFF parameters have been developed in our previous work.[38–41] In this work, LiTFSI with EC solvents are used to clarify the reduction mechanism, formation process, and main components of the SEI layer. Further investigation is conducted with different LiTFSI concentrations to achieve the controlled SEI layer formation process along with radial distribution function (RDF), X-ray diffraction (XRD), and X-ray photoelectron spectroscopy (XPS) analysis method.

2. Results and Discussion

2.1. Initial Reductive Reaction of EC from HAIR Simulation

According to HAIR simulation results, we reproduced the initial degradation reduction mechanisms of EC and LiTFSI and compared them with previous work to obtain reliable initial reaction results within 22 ps.[22,33,34,42] **Figure 1** exhibits the initial decomposition pathway for EC. It shows that EC undergoes two reaction processes as predicted by Camacho-Forero.[22] EC accepts one electron to form EC^- ion, and the electron transfer is very fast, as mentioned by Leung using constrained DFT (cDFT) approach.[43] Subsequently, EC^- ion experiences two pathways. EC^- ion accepts another electron and decomposes into CO_3^{2-} and C_2H_4, observed experimentally.[35] Concerning the other pathway, the reaction process exhibits more complex and multi-step processes, EC^- ion undergo C-O bond breaking with $OC_2H_4OCO^-$ formed, $OC_2H_4OCO^-$ is reduced by accepting one electron with the release of CO, while $OC_2H_4OCO^-$ could also release CO_2 via a homolytic reaction and generate an ethylene oxide radical anion $\bullet CH_2CH_2O^-$, which is also mentioned by Jin.[35] Obviously, it is a remarkable fact that $\bullet CH_2CH_2O^-$ is more reactive than $OC_2H_4O^{2-}$, to initiate further reactions from $\bullet CH_2CH_2O^-$, The Gibbs free energies (**Table 1**) of these pathways are calculated at B3LYP/6-311+g(d,p) level using Jaguar 8.8. For example, CO_2 attacks the C-atom in $\bullet CH_2CH_2O^-$ to form $OC_2H_4CO_2^{2-}$ along with accepting one electron, and CO attacks the O-atom to generate CO_2 and C_2H_4 and one electron transfer to solvent EC simultaneously. Besides, recombination reactions are also seen during HAIR simulations, the combination of C_2H_4 and $\bullet CH_2CH_2O^-$ to produce $C_2H_4C_2H_4O^-$. In addition, $\bullet CH_2CH_2O^-$ attacks another EC^- ion via a ring-opening process to release CO_2 and $OC_2H_4C_2H_4O^{2-}$, which Jin also proposes as the initial anionic polymerization process according to experimental results.[35]

Table 1. The Gibbs free energies (kcal mol^{-1}) of four pathway from •$CH_2CH_2O^-$ at B3LYP/6-311+g(d,p) level.

Reaction	Gibbs free energies [kcal mol^{-1}]
•$CH_2CH_2O^-$ + e + CO_2 = $OC_2H_4CO_2^{2-}$	ΔG = -19.7 kcal mol^{-1}
•$CH_2CH_2O^-$ + EC^- = $OC_2H_4C_2H_4O^{2-}$ + CO_2	ΔG = -11.5 kcal mol^{-1}
•$CH_2CH_2O^-$ + CO + EC = EC^- + C_2H_4 + CO_2	ΔG = -36.4 kcal mol^{-1}
•$CH_2CH_2O^-$ + C_2H_4 = $OC_2H_4C_2H_4^-$	ΔG = -9.2 kcal mol^{-1}

Figure 2 shows the further reactions of $OC_2H_4CO_2^{2-}$, the molecule of $OC_2H_4CO_2^{2-}$ is reduced by Li^0 to form Li_2O through the oxygen removal process, and the following step is the C—C bond cleavage of OC_2H_4CO with CH_2O and CH_2CO formed. These two molecules could experience two reaction processes, including recombination and hydrogen exchange reactions, which finally contribute to an organic layer of SEI film by Li coordination. The initial reductive reaction processes from EC obtained from HAIR simulations are validated by previous theoretical and experimental work and extend the further recombination reaction, which provides more insights to get a comprehensive understanding of SEI formation.

2.2. Distributions of Reductive Reactions within 22.0 ps

Based on the initial reaction mechanism of EC, we explored the distributions of reductive reaction pathways within 4 cycles (22 ps), as shown in **Figure 3**. During 0–5.5 ps, only one molecule EC in 14 molecules decomposes to form $OC_2H_4CO_2^{2-}$. Most EC molecules experience further decomposition reaction to release CO at 6.0 ps. Concerning the HAIR simulation within 22 ps, we found that the EC molecules mainly decompose into $OC_2H_4O^{2-}$ or •$CH_2CH_2O^-$, which are in accordance with theoretical results reported by Camacho-Forero.[22] The sequence of LiTFSI decomposition obtained from HAIR simulation between 0–50.0 ps is exhibited in Figure S2 (Supporting Information). Accordingly, the decomposition of TFSI is initiated by N—S bond cleavage to form NSO_2CF_3 and SO_2CF_3 fragments at 5.5 ps, consistent with previous theoretical results.[38,44–46]

2.3. Organic and Inorganic Parts of the SEI Layer

Based on the initial reduction of electrolyte at the Li metal anode surface, long-time simulations are extended to be 1 ns, including

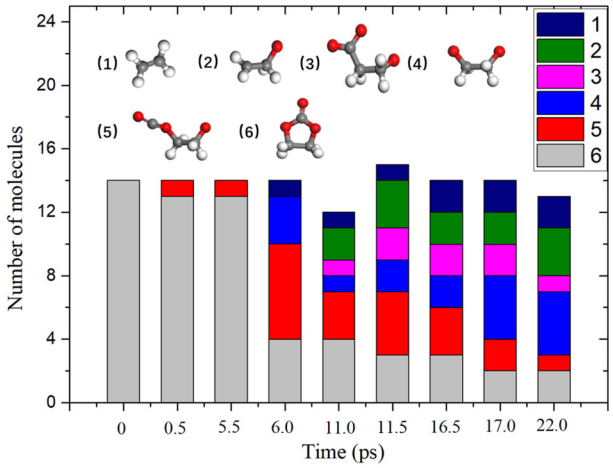

Figure 3. The number of EC decomposition molecules obtained from HAIR simulations within 22 ps.

550 ps HAIR simulation with 450 ReaxFF and 10 ps AIMD simulations. The theoretical results are shown in **Figure 4**, two parts of the SEI layer could be clarified. Figure 4a shows the organic parts of the SEI layer, long-chain oligomers were observed, which derives from the reduction of EC solvent as mentioned in Figures 1 and 2. In **Table 2**, the products in the organic part contain different linear polyethylene oxide (PEO) species, i.e., R-OCH_2CH_2O- and R'-OCH_3 groups, which is observed by Jin[35] with solid-state nuclear magnetic resonance (NMR) techniques, indicating a reliable composition of SEI layer simulated with HAIR simulations. Moreover, $Li_2OCO_2CH_2CH_2$ and $Li_2OCO_2(CH_2)_4$ are seen in the organic part, showing good agreements with work reported by Bedrov.[33] Further organic sulfur-contained compounds are also clarified due to the decomposition of LiTFSI. The geometries of organic products in Table 2 are shown in Figure S3 (Supporting Information). As for the inorganic parts exhibited in Figure 4b, the main products are LiF, LiOH, Li_2O, and LiOCN, along with C_2H_4 and CH_4 gas products, as observed in experiments.[30,35]

After long-time simulations, the detailed reaction mechanism is investigated to clarify the organic products further. **Figure 5**a–f exhibits the organic products formation process sequence. During 231 and 467.5 ps, the recombination processes of CO_2, CH_2O^- and C_2O are observed to form $OCH_2C(CO)C(O)CH_2O^{2-}$ as shown in Figure 5e. Subsequently, $OCH_2C(CO)C(O)CH_2O^{2-}$ experiences H-atom transfer and CO_2 attacking reactions, forming $Li_2C_6O_6H_4$. Figure 5g–l shows the sequence of $C_{11}H_{11}SO_5^{2-}$,

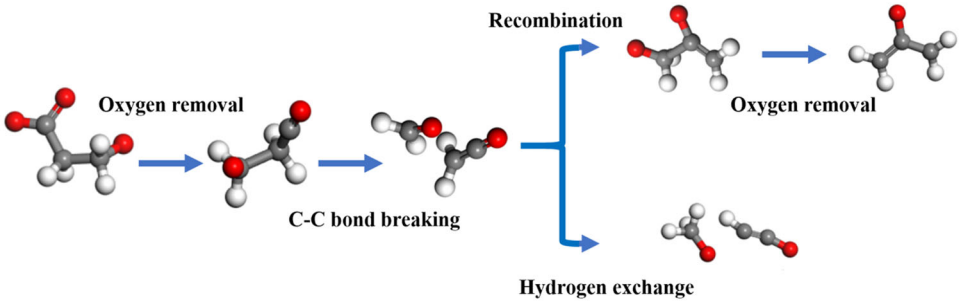

Figure 2. Initial reductive reaction pathways of $OC_2H_4CO_2^{2-}$ obtained from HAIR simulations.

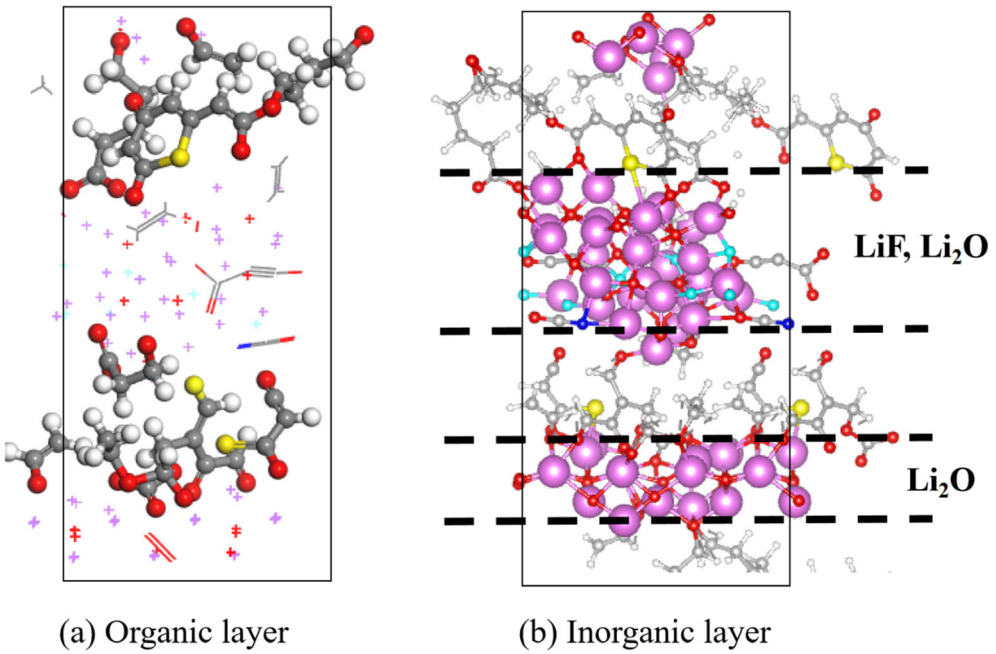

Figure 4. Snapshots from MD simulation after 1 ns. a) Organic parts, b) Inorganic parts. Color code: lithium, purple, oxygen, red, carbon, gray, fluorine, cyan, sulfur, yellow, nitrogen, blue.

Table 2. The organic and inorganic parts of the SEI layer obtained from MD simulations.

	Main products
Inorganic part	LiF, Li_2O, LiOH, LiOCN
Organic part	$LiOC_2H_3$, $Li_2OCO_2CH_2CH_2$, $Li_2OCO_2(CH_2)_4$, $LiOCH_2OCH_2CH_3$, $LiO(CH_2)_2OLi$, $Li_2C_6O_6H_4$, $LiOCSC_2OH$, $Li_3C_{11}H_{11}SO_5$.

sulfur atom attacks the $OCH_2CH_2CO^{2-}$ to imitate the polymerization process by forming $OCH_2CH_2COS^{2-}$. During 385 and 445.5 ps, the $OCH_2CH_2COS^{2-}$ undergo multi-step ring-closure and opened reactions and finally form a six-member ring as in Figure 5k. Finally, the $O(CH_2)_4O^{2-}$ attacks the carbon-atom in a six-member ring along with electron transfer to generate $C_{11}H_{11}SO_5^{3-}$.

2.4. Organic and Inorganic Parts of the SEI Layer

The strategies proposed to inhibit dendrite growth and improve the CEs by developing high concentration (HC) electrolytes. We investigate the formation process and components of the SEI layer with different concentrations of Li-salts. For the sake of getting a reliable initial reaction between Li-slab and electrolyte, we conducted the AIMD simulations for 1 and 5 M concentrations LiTFSI/EC systems, and the initial models could be found in Supporting Information. **Figure 6** exhibited the snapshots from AIMD simulations at 20 ps. We found that the EC molecule in the 1 M concentration system undergoes two processes as same as HAIR results, which are C_2H_4, Li_2CO_3, and ring-opened EC through one- and two-electrons mechanisms. As the reaction shown in HC electrolyte, no decomposition of EC is observed while the LiTFSI reduced to protect EC solvents, showing differences with low concentration electrolyte, denoted as sacrificial reduction mechanism proposed by Sodeyama.[45]

Figure 7 exhibits the snapshots from MD simulations after 1 ns. Significant differences for the structure and components of the SEI layer could be identified with radial distribution function (RDF) and X-ray photoelectron spectroscopy (XPS) analyses. In Figure 7, a homogenous and stable SEI layer is formed at a 5 M concentration. At the same time, multilayer SEI, comprised of liner PEO species and inorganic pars, is shown in the 1M LiTFSI/EC system, which provides new insights for SEI morphology evolution. RDF and XPS results (shown in Figures S4 and S5, Supporting Information) imply the salt-derived SEI composition at 5 M concentration systems, mainly consisting of LiF or Li_2O.

The extended time scale via HAIR scheme allows the direct observation of oligomer reactions. Such a process is expected to propagate to create polymers in SEI, which might be better characterized using larger-scale simulations utilizing ReaxFF or other molecular dynamics that can model chemical/electrochemical processes, rather than the two hundred atoms simulation in the work.[47] The diffusion of Li^+ in SEI has been recognized as great importance, but still puzzling. Various diffusion mechanisms have been proposed based on theory and experiment.[48]

One of the advantages of HAIR is the explicit consideration of solvation, especially in such complex reaction conditions as SEI. Nevertheless, the current limitation comes from the limited size that can be accessed in simulation because of the expensive AIMD part. Further research toward totally replacing AIMD with a machine learning potential that is more accurate than ReaxFF is underway.

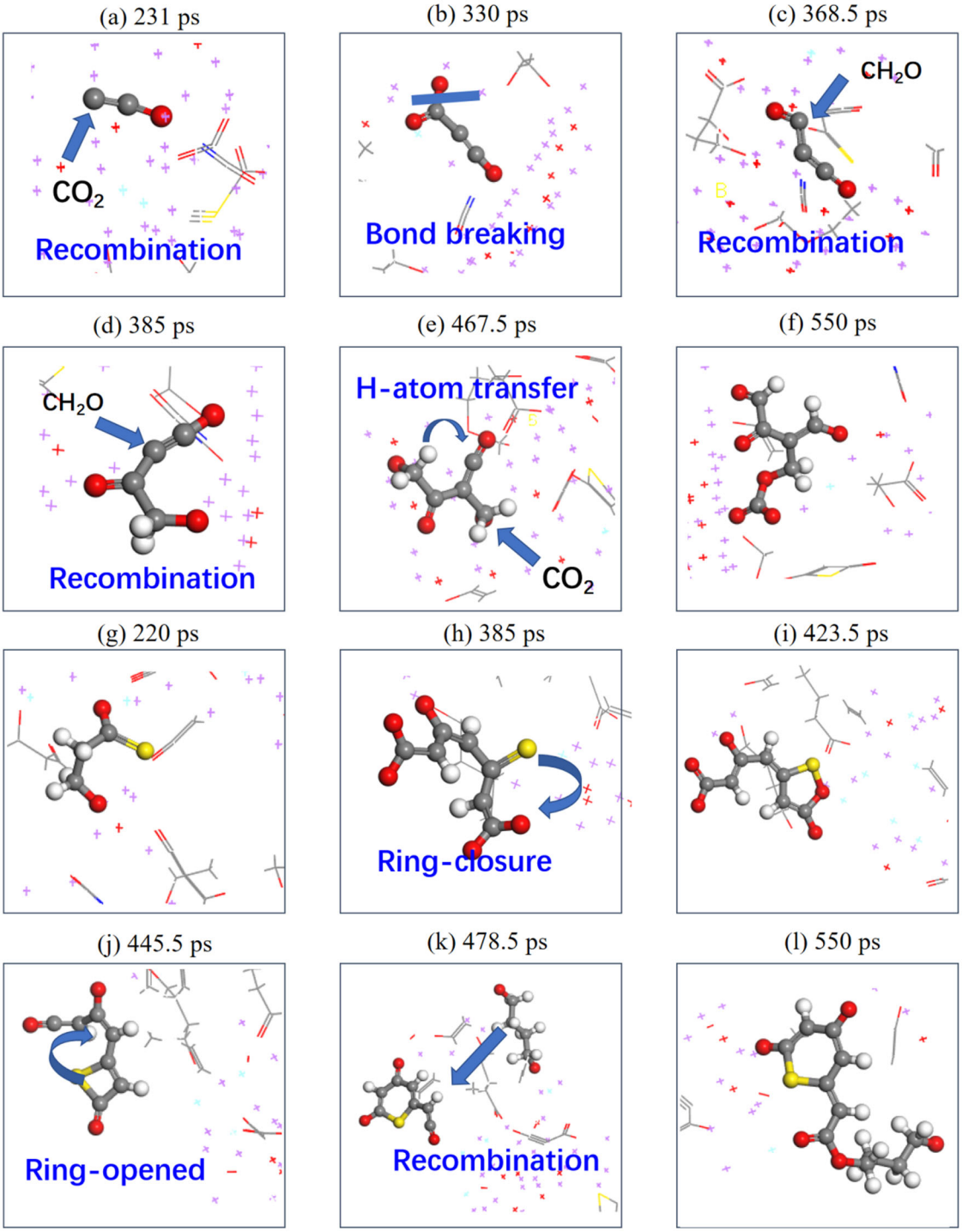

Figure 5. The sequence of the formation process for organic products a–f) $C_6O_6H_4^{2-}$ and g–l) $C_{11}H_{11}SO_5^{3-}$ during 220–550 ps. Color code: lithium, purple, oxygen, red, carbon, gray, fluorine, cyan, sulfur, yellow, nitrogen, blue.

3. Conclusions

In summary, a hybrid scheme (HAIR), combining ab initio and reactive force field reactive dynamics, is used to explore the reduction mechanism toward SEI formation of LiTFSI/EC electrolyte (1 and 5 M concentrations) with Li metal anode. Detailed initial reductive mechanisms of EC and LiTFSI are distinguished from the HAIR MD reactive trajectories, revealing that EC molecule mainly reduced via two-electron ($2e^-$) reaction to $OC_2H_4O^{2-}$ or $\bullet CH_2CH_2O^-$. Such predictions well agree with the previous AIMD results reported by Camacho-Forero.[22] The simulation is then extended to 1 ns with the help of HAIR

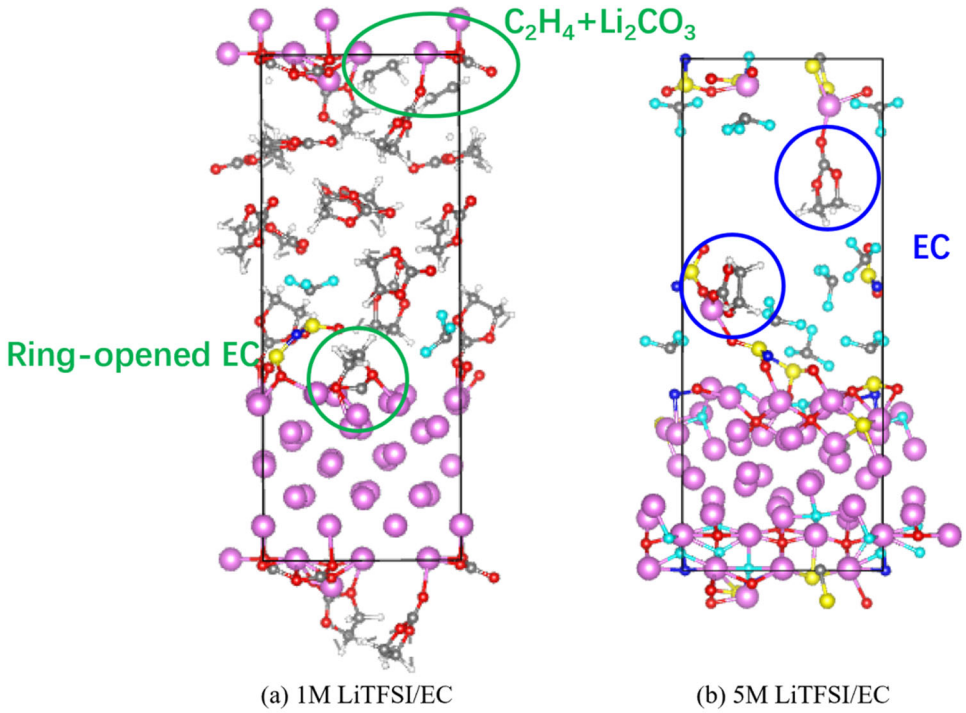

Figure 6. Snapshots from AIMD simulation at initial 20 ps. a) 1 M LiTFSI/EC, b) 5 M LiTFSI/EC. Color codes as shown in Figure 4.

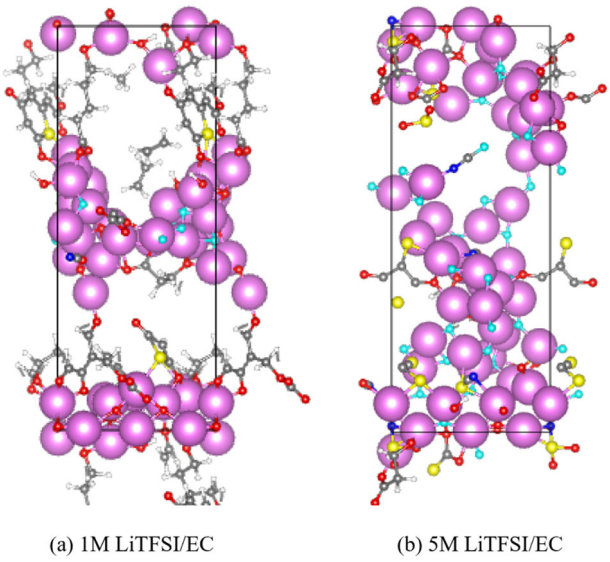

Figure 7. Snapshots from MD simulation after 1 ns simulation. a) 1 M LiTFSI/EC, b) 5 M LiTFSI/EC. Color codes as shown in Figure 4.

to investigate deep products over a longer time scale. Distinct inorganic components of LiF and Li_2O that make up the inner inorganic layer (IIL) and organic components of $Li_2OCO_2CH_2CH_2$ and $Li_2OCO_2(CH_2)_4$ that make up the outer organic layer (OOL) are developed in HAIR simulation. As simulation time increases, reactive intermediates in OOL further polymerize into linear PEO oligomers, which has been mentioned in experimental[35] and theoretical[33] research but has never been confirmed. RDF and XPS analysis further reveal the difference in SEI between 1 and 5 M electrolytes, demonstrating that homogenous LiF in IIL of SEI layer is formed at 5 M electrolyte, but not in 1 M electrolyte although F releasing also occurs. The aforementioned extensive information on the reduction mechanism and morphological evolution toward the SEI formation process, derived from long-term hybrid simulations, provides atomic insight for accelerating the development of advanced electrolytes.

4. Experimental Section

Simulated Models: In order to represent the LiTFSI/EC system, 14 EC molecules with 1 LiTFSI molecule were placed in a 10.5 × 10.5 × 26.5 Å periodic box to achieve the desired 1 M concentration of Li-salts in the electrolyte. The Li-metal anode was represented by a 6-layer (3 × 3) supercell slab, where two of the bottom layers of the slab were fixed (Figure S1, Supporting Information) with the most stable Li (100) surface. To achieve the desired concentrations of Li-salts in the electrolyte, 1 and 5 molecules LiTFSI dissolved in EC solvents were used to represent 1 and 5 M LiTFSI/EC electrolyte systems.

The Workflow of HAIR Simulation: The workflow of HAIR requires AIMD and RMD simulations alternatively after a geometry optimization using DFT method. In the initial reactions, each battery cycle includes 0.5 ps AIMD and 5.0 ps RMD simulations with a 10-time acceleration to guarantee reliable chemical reaction. After 450 HAIR simulation, the new reactions were rare, which suggest an increase of acceleration rate to 100 times. After finishing the 1 ns HAIR simulation, a 10 ps AIMD was carried out to product trajectory for further analysis such as prediction of vibrations.

Computational Details for AIMD Simulation: To perform the HAIR method, the AIMD procedure was simulated using the Vienna ab Initio Simulation Package (VASP 5.4.4),[49] which lasts 0.5 ps for one cycle, and the timestep was chosen as 1 fs. Perdew–Burke–Ernzerhof (PBE)

functional describes the electron exchange and correction energies within the generalized gradient approximation (GGA).[50] Moreover, the Grimme D3 correction was added to describe the London dispersion integrations.[51] The projector augmented wave (PAW) method implemented in VASP was utilized.[52] As for sampling Brillouin zone integration, [53] a $1 \times 1 \times 1$ Monkhorst-Pack k-point mesh was used, and a 400-eV energy cutoff was chosen as plane-wave basis expansion. To obtain the reliable AIMD results, 0.2 eV width of Gaussian smearing and 10^{-4} eV for electronic structure convergence of the self-consistent field are used in this work.

Computational Details for ReaxFF Simulation: Concerning the ReaxFF simulations, the Large-scale Atomic/Molecular Massively Parallel Simulator (LAMMPS 2018)[54] software was used to conduct 5 ps long simulation for one cycle in the HAIR method. To guarantee good energy conservation while ensuring efficient convergence for collisions and smooth reactions, a proper 0.25 fs timestep is chosen in this work. And NVT ensemble at 300 K, which fixes the molecule numbers (*N*), volume (*V*), and temperature (*T*), were employed during HAIR simulations.

Supporting Information

Supporting Information is available from the Wiley Online Library or from the author.

Acknowledgements

T.C. thanks the support from Collaborative Innovation Center of Suzhou Nano Science & Technology, the Priority Academic Program Development of Jiangsu Higher Education Institutions (PAPD), the 111 Project, Joint International Research Laboratory of Carbon-Based Functional Materials and Devices, the National Natural Science Foundation of China (21903058 and 22173066), the Natural Science Foundation of Jiangsu Province (BK20190810), the Jiangsu Province High-Level Talents (JNHB-106). The authors thank Wenxuan Du for his useful discussions.

Conflict of Interest

The authors declare no conflict of interest.

Data Availability Statement

The data that support the findings of this study are available in the supplementary material of this article.

Keywords

hybrid molecular dynamics, linear oligomers, lithium metal batteries, reduction mechanism, solid electrolyte interphase

Received: December 18, 2021
Revised: February 1, 2022
Published online:

[1] J. B. Goodenough, K. S. Park, *J. Am. Chem. Soc.* **2013**, *135*, 1167.
[2] W. Xu, J. Wang, F. Ding, X. Chen, E. Nasybulin, Y. Zhang, J. G. Zhang, *Energy Environ. Sci.* **2014**, *7*, 513.
[3] D. Lin, Y. Liu, Y. Cui, *Nat. Nanotechnol.* **2017**, *12*, 194.
[4] X. B. Cheng, R. Zhang, C. Z. Zhao, Q. Zhang, *Chem. Rev.* **2017**, *117*, 10403.
[5] J. M. Zheng, M. H. Engelhard, D. H. Mei, S. H. Jiao, B. J. Polzin, J. G. Zhang, W. Xu, *Nat. Energy* **2017**, *2*, 17012.
[6] C. Huang, J. Xiao, Y. Shao, J. Zheng, W. D. Bennett, D. Lu, L. V. Saraf, M. Engelhard, L. Ji, J. Zhang, et al., *Nat. Commun.* **2014**, *5*, 3015.
[7] F. Shi, A. Pei, D. T. Boyle, J. Xie, X. Yu, X. Zhang, Y. Cui, *Proc. Natl. Acad. Sci. U. S. A.* **2018**, *115*, 8529.
[8] J. Scheers, S. Fantini, P. Johansson, *J. Power Sources* **2014**, *255*, 204.
[9] F. Ding, W. Xu, X. Chen, J. Zhang, M. H. Engelhard, Y. Zhang, B. R. Johnson, J. V. Crum, T. A. Blake, X. Liu, et al., *J. Electrochem. Soc.* **2013**, *160*, A1894.
[10] K. Xu, *Chem. Rev.* **2014**, *114*, 11503.
[11] S. Li, M. Jiang, Y. Xie, H. Xu, J. Jia, J. Li, *Adv. Mater.* **2018**, *30*, 1706375.
[12] K. Yoshida, M. Nakamura, Y. Kazue, N. Tachikawa, S. Tsuzuki, S. Seki, K. Dokko, M. Watanabe, *J. Am. Chem. Soc.* **2011**, *133*, 13121.
[13] Y. Jie, X. Ren, R. Cao, W. Cai, S. Jiao, *Adv. Funct. Mater.* **2020**, *30*, 1910777.
[14] I. M. Markus, G. Jones, J. M. Garcia, *J. Phys. Chem. C* **2016**, *120*, 5949.
[15] Y. Yamada, M. Yaegashi, T. Abe, A. Yamada, *Chem. Commun.* **2013**, *49*, 11194.
[16] X. Q. Zhang, X. Chen, X. B. Cheng, B. Q. Li, X. Shen, C. Yan, J. Q. Huang, Q. Zhang, *Angew. Chem., Int. Ed.* **2018**, *57*, 5301.
[17] X. B. Cheng, R. Zhang, C. Z. Zhao, F. Wei, J. G. Zhang, Q. Zhang, *Adv. Sci.* **2016**, *3*, 1500213.
[18] A. Wang, S. Kadam, L. Li, S. Shi, Y. Qi, *npj Comput. Mater.* **2018**, *4*, 15.
[19] K. Leung, *Phys. Chem. Chem. Phys.* **2015**, *17*, 1637.
[20] X. Fan, L. Chen, X. Ji, T. Deng, S. Hou, J. Chen, J. Zheng, F. Wang, J. Jiang, K. Xu, C. Wang, *Chem* **2018**, *4*, 174.
[21] S. Q. Shi, J. Gao, Y. Liu, Y. Zhao, Q. Wu, W. J. Wang, C. Y. Ouyang, R. J. Xiao, *Chin. Phys. B* **2016**, *25*, 018212.
[22] Q. He, B. Yu, Z. H. Li, Y. Zhao, *Energy Environ. Mater.* **2019**, *2*, 264.
[23] Y. X. Wang, S. Nakamura, M. Ue, P. B. Balbuena, *J. Am. Chem. Soc.* **2001**, *123*, 11708.
[24] S. P. Beltran, X. Cao, J. G. Zhang, P. B. Balbuena, *Chem. Mater.* **2020**, *32*, 5973.
[25] L. E. Camacho-Forero, T. W. Smith, P. B. Balbuena, *J. Phys. Chem. C* **2017**, *121*, 182.
[26] L. E. Camacho-Forero, P. B. Balbuena, *J. Power Sources* **2020**, *472*, 228449.
[27] S. P. Kim, A. C. T. van Duin, V. B. Shenoy, *J. Power Sources* **2011**, *196*, 8590.
[28] K. Leung, *J. Phys. Chem. C* **2013**, *117*, 1539.
[29] X. Teng, C. Zhan, Y. Bai, L. Ma, Q. Liu, C. Wu, F. Wu, Y. Yang, J. Lu, K. I.n Amine, *ACS Appl. Mater. Interfaces* **2015**, *7*, 22751.
[30] A. C. T. van Duin, S. Dasgupta, F. Lorant, W. A. R. F. F. Goddard, *J. Phys. Chem. A* **2001**, *105*, 9396.
[31] K. Chenoweth, A. C. T. van Duin, W. A. Goddard, *J. Phys. Chem. A* **2008**, *112*, 1040.
[32] D. Bedrov, G. D. Smith, A. C. T. van Duin, *J. Phys. Chem. A* **2012**, *116*, 2978.
[33] K.-S. Yun, S. J. Pai, B. C. Yeo, K.-R. Lee, S.-J. Kim, *J. Phys. Chem. Lett.* **2017**, *8*, 2812.
[34] Y. Jin, N. H. Kneusels, P. M. M. M. Magusin, G. Kim, E. Castillo-Martinez, L. E. Marbella, R. N. Kerber, D. J. Howe, S. Paul, T. Liu, C. P. Grey, *J. Am. Chem. Soc.* **2017**, *139*, 14992.
[35] K. A. O'Hearn, M. W. Swift, J. Liu, I. Magoulas, P. Piecuch, A. C. T. van Duin, H. M. Aktulga, Y. Qi, *J. Chem. Phys.* **2020**, *153*, 084107.
[36] M. M. Islam, G. Kolesov, T. Verstraelen, E. Kaxiras, van Duin, A. C. T. eReaxFF, *J. Chem. Theory Comput.* **2016**, *12*, 3463.
[37] Y. Liu, P. P. Yu, Y. Wu, H. Yang, M. Xie, L. Y. Huai, W. A. Goddard, T. Cheng, *J. Phys. Chem. Lett.* **2021**, *12*, 1300.
[38] Y. Liu, Q. T. Sun, P. P. Yu, Y. Wu, L. Xu, H. Yang, M. Xie, T. Cheng, W. A. Goddard, *J. Phys. Chem. Lett.* **2021**, *12*, 2922.
[39] Y. Liu, Q. T. Sun, Y. Wu, M. Xie, H. Yang, T. Cheng, W. A. Goddard, *ACS Energy Lett.* **2021**, *6*, 2320.

[40] Y. Liu, Q. T. Sun, P. P. Yu, B. Y. Ma, H. Yang, J. Y. Zhang, M. Xie, T. I.n Cheng, *J. Mater. Chem. A* **2022**, *10*, 632.
[41] G. Kresse, J. Hafner, *Phys. Rev. B: Condens. Matter Mater. Phys.* **1994**, *49*, 14251.
[42] K. Leung, Y. Qi, K. R. Zavadil, Y. S. Jung, A. C. Dillon, A. S. Cavanagh, S. H. Lee, S. M. George, *J. Am. Chem. Soc.* **2011**, *133*, 14741.
[43] E. P. Kamphaus, S. Angarita-Gomez, X. Qin, M. Shao, M. Engelhard, K. T. Mueller, V. Murugesan, P. B. Balbuena, *ACS Appl. Mater. Interfaces* **2019**, *11*, 31467.
[44] K. Sodeyama, Y. Yamada, K. Aikawa, A. Yamada, Y. Tateyama, *J. Phys. Chem. C* **2014**, *118*, 14091.
[45] B. V. Merinov, S. V. Zybin, S. Naserifar, S. Morozov, J. Oppenheim, W. A. Goddard, J. Lee, J. H. Lee, H. E. Han, Y. C. Choi, *J. Phys. Chem. Lett.* **2019**, *10*, 4577.
[46] G. R. Gissinger, B. D. Jensen, K. E. Wise, *Polymer* **2017**, *128*, 211e217.
[47] S. Q. Shi, P. Lu, Z. Y. Liu, Y. Qi, L. G. Hector Jr., H. Li, S. J. Harris, *J. Am. Chem. Soc.* **2012**, *134*, 15476.
[48] H. Yanxon, D. Zagaceta, B. Tang, D. S. Matteson, Q. Zhu, *Mach. Learn.: Sci. Technol.* **2021**, *2*, 027001.
[49] J. P. Perdew, K. Burke, M. Ernzerhof, *Phys. Rev. Lett.* **1996**, *77*, 3865.
[50] S. Naserifar, J. J. Oppenheim, H. Yang, T. Zhou, S. Zybin, M. Rizk, W. A. Goddard, *J. Chem. Phys.* **2019**, *151*, 154111.
[51] G. Kresse, D. Joubert, *Phys. Rev. B: Condens. Matter Mater. Phys.* **1999**, *59*, 1758.
[52] H. J. Monkhorst, J. D. Pack, *Phys. Rev. B* **1976**, *13*, 5188.
[53] S. Plimpton, *J. Comput. Phys.* **1995**, *117*, 1.
[54] Y. Wang, Y. Liu, Y. Tu, Q. Wang, *J. Phys. Chem. C* **2020**, *124*, 9099.